

This is the peer reviewed version of the following article:

Sand liquefaction induced by a blast test: New insights on source layer and grain-size segregation mechanisms (Late Quaternary, Emilia, Italy) / Fontana, Daniela; Amoroso, Sara; Minarelli, Luca; Stefani, Marco. - In: JOURNAL OF SEDIMENTARY RESEARCH. - ISSN 1527-1404. - 89:1(2019), pp. 13-27. [10.2110/jsr.2019.1]

Terms of use:

The terms and conditions for the reuse of this version of the manuscript are specified in the publishing policy. For all terms of use and more information see the publisher's website.

14/07/2024 08:58

(Article begins on next page)

1

2 Sand liquefaction induced by a blast test: new insights on source layer and grain-size segregation
3 mechanisms (Late Quaternary, Emilia, Italy)

4

5 Daniela Fontana¹, Sara Amoroso², Luca Minarelli³ and Marco Stefani⁴

6

7 ¹ *Department of Chemical and Geological Sciences, University of Modena and Reggio*

8 *Emilia, Modena, Italy*

9 ² *Istituto Nazionale di Geofisica e Vulcanologia, L'Aquila, Italy*

10 ³ *Geotema s.r.l. Spin-off University of Ferrara, Italy*

11 ⁴ *Department of Architecture, University of Ferrara, Italy*

12 *e-mail: daniela.fontana@unimore.it*

13

14

ABSTRACT

15

16 The composition and texture of liquefied sands represent an important tool for the recognition of
17 buried source layers and for a better understanding of earthquake-induced liquefaction mechanisms.

18 The earthquake-simulating field experiment (blast test) carried out in 2016 in fluvial sediments of
19 the Emilia plain induced subsurface liquefaction and the surface expulsion of sand as sand blows.

20 The area was widely affected by liquefaction phenomena during the Mw 6.1 Emilia earthquake
21 (2012). The grain size and composition of sand blows ejected during the blast test have been

22 compared with various horizons of buried fluvial sediments as deep as 20 m, and with sands from
23 two trenches in the blast site representative of co-seismic 2012 liquefied sands. The sands from the

24 cores show a clear trend from shallow lithoarenitic to deeper quartz–feldspar-rich compositions.

25 The sands at shallow depth (up to 7.7 m) are the most lithoarenitic, with fine-grained sedimentary
26 rock fragments (shales, siltstones, and limestone) as the dominant lithic type. Lithic fragments

1 derive mostly from erosion of sedimentary terrigenous and carbonate successions of Apenninic
2 affinity. In contrast, deeper sands (at depth > 7.7 m) are enriched in quartz and feldspars and
3 impoverished in lithic fragments, which are similar in character to Po River sands. The composition
4 of ejected sands largely overlap that of the shallow litharenitic Apenninic sands, indicating that
5 liquefaction processes affected mainly sand layers at relatively shallow depth (5.9–7.7 m). Textural
6 parameters show that silty sands and silts characterized by relatively high content of fines can also
7 liquefy. This is in contrast to most of the literature, where fine-grained sediments are considered as
8 incapable of generating the high pore pressures commonly associated with liquefaction. This result
9 should be considered when estimating the liquefaction as a potential hazard. Moreover, we observe
10 that there is a selective loss of fines in the clastic dikes and sand volcanoes relative to the source
11 beds, indicating that the liquefaction process appears to preferentially select the diameters of the
12 grains that reach the ground surface, probably following the generated excess pore-water pressure.
13 This may have caused the segregation and dispersion of the fine silt–clay content, producing highly
14 sorted sand boils. This effect is well observable in both the blast-induced sand boils, and the co-
15 seismic 2012 dikes and sand boils ejected in the same area.

16

17

18 Keywords: silty sand liquefaction, blast test, provenance, fluvial sands, Emilia earthquake

19

20

21

INTRODUCTION

22

23 Extensive liquefaction phenomena of fluvial sands buried in the shallow subsurface have
24 occurred in the central-eastern sector of the Po plain, following the two main shocks (M_L 5.8 and
25 5.9) of the 2012 Emilia earthquake. The ejection of liquefied sands through fractures to the

1 surface has generated numerous sand boils, concentrated along buried old channels of Apenninic
2 rivers (Fig. 1).

3 It is well known that the occurrence of sand liquefaction phenomena may cause significant
4 modifications of soil geotechnical properties and reduction of load-bearing capacity, with
5 potential destruction and damages to structures and even human casualties. It is therefore crucial
6 to improve the understanding of the factors that may induce liquefaction (Krinitzsky et al., 1988;
7 Mitchell and Soga, 2005; Chen et al., 2008). Some of these factors, such as earthquake
8 magnitude, depth of the groundwater table, peak ground acceleration, and sediment grain size,
9 are relatively well defined (Youd and Perkins, 1978; Ishihara, 1993; Kramer, 1996; Bray and
10 Sancio, 2006; Chang et al., 2011) although simplified models of soils are used. However, little is
11 known about other relevant geological parameters, in particular sedimentary facies and lateral
12 facies changes, and changes in texture and composition of sediment in liquefiable layers. Recent
13 papers have shown the potential of detailed sedimentological studies for the comprehension of
14 liquefaction processes (Hurst et al., 2011; Owen and Moretti, 2011; Ross et al., 2011, 2013;
15 Quigley et al., 2013; Fontana et al., 2015; Rodriguez Pasqua et al., 2015; Amorosi et al., 2016;
16 Cobain et al., 2017; Giona Bucci et al., 2017). The composition of sand dikes and blows
17 represents an important tool to identify the liquefied source layers in the subsurface, while
18 sedimentary structures and texture may provide information on pulse injection mechanisms of
19 liquefied sands along fractures (Nichols et al., 1994; Hurst et al., 2011; Ross et al., 2014;
20 Fontana et al., 2015).

21 Physical experiments in New Zealand and in the United States have shown that liquefaction
22 can be induced and monitored with field-scale blast tests in order to study the associated effects
23 on soil characteristics (Ashford et al., 2004; Rollins et al., 2004; Wentz et al., 2015; Finno et al.,
24 2016). Following these experiments, in 2016 a research project on blast-induced liquefaction at
25 the field scale was performed at a trial site located in Mirabello (Ferrara, Italy; Amoroso et al.,
26 2017) (Fig. 1), a small town strongly affected by liquefaction phenomena during the 2012 Emilia

1 earthquake (Caputo and Papathanasiou, 2012; Emergeo Working Group, 2013; Fioravante et al.,
2 2013). The stratigraphical, geotechnical, and geophysical properties at the test site were
3 investigated in detail, through several multidisciplinary techniques (Amoroso et al., 2017). Two
4 cores (10 and 20 m deep) and two shallow trenches in the test site allowed to reconstruct the
5 stratigraphy of sediments in the subsurface and the sampling of sands.

6 Here, the composition of sand blows ejected during the blast test, compared with the
7 composition of different horizons of buried fluvial sediments as deep as 20 m, has proved to be
8 an important tool to identify the liquefied layers. Moreover, for the first time the sands involved
9 into the blast-test experiment are characterized by a relatively high fine-grained content
10 compared with previous blast experiences performed in cleaner sands. This has allowed a better
11 understanding of the selective processes undergone by sediments during the ejection.

12

13

14

GEOLOGICAL SETTING

15

16 The Po Plain represents the sedimentary filling of the Apennine foredeep, made up of a thick
17 succession of Miocene–Quaternary marine and continental deposits. Beneath the alluvial plain,
18 the fault–fold structures of the external portion of the Apenninic orogenic wedge are buried
19 (Boccaletti et al., 2004; Ghielmi et al., 2013). Buried anticlines formed mainly during the
20 Cenozoic in response to the collision between the European and the Adria plates (Ricci Lucchi,
21 1986; Argnani et al., 2006). The ongoing deformation of the buried fault–fold structures,
22 superimposed on a fast regional subsidence affecting mainly the southern portion of the foredeep
23 basin (Carminati et al, 2005) allowed a thick accumulation of fluvial sediments, primarily due to
24 the Po River and multiple Apenninic tributaries. The thickness of the sedimentary infill is highly
25 variable, from 4 km in depocenter area, close to the Apenninic mountain front, to a few hundred

1 meters in correspondence of the buried anticlines (Mariotti and Doglioni, 2000; Ghielmi et al,
2 2013).

3 The thick Quaternary successions are punctuated by several unconformities controlled by the
4 glacio-eustatic transgressive–regressive fluctuations (Amorosi et al, 2008; Garzanti et al, 2011),
5 supporting the subdivision of the succession into allostratigraphic units. The sediments discussed
6 in this research are ascribed to the last depositional cycle, referable to the upper portion of the
7 Villa Verrucchio Subsynthem (AES7) and the Ravenna Subsynthem (AES8) (Fig. 2). The two
8 units, here consisting entirely of fluvial sediments, are separated by a regional discontinuity
9 surface marked by widespread organic-rich and weakly developed paleosoils (Stefani et al.,
10 2018).

11 In the study area, the upper portion of the Villa Verrucchio Subsynthem (AES7) is dominated
12 by sands accumulated during the Last Glacial Maximum (LGM). The Ravenna Subsynthem
13 (AES8) is made up of silt, silty clay, organic-rich clay, and peats recording wide continental
14 swamps intercalated with sands and silty sands deposited into fluvial channel and levee settings
15 by various rivers. The upper portion of the AES8 is dominated by the large sand body of the
16 Reno River, flanked by its levee and by interfluvial depression deposits (Stefani et al., 2018).

17 The region is affected by significant seismic activity due to the compressional deformation of
18 fault–fold structures of the buried orogenic wedge. In May 2012, a severe seismic sequence
19 induced significant human casualties, diffuse damage of buildings, and widespread liquefaction
20 of fluvial sand and silt bodies, buried in the shallow subsurface (Caputo and Papathanasiou,
21 2012; Emergeo Working Group, 2013; Fioravante et al., 2013). An area severely affected by the
22 liquefaction phenomena has been the southwestern portion of the Ferrara Province, at San Carlo
23 and Mirabello, which is the object of this study (Fig. 1).

24

25

26

MATERIALS AND METHODS

1

2 **Blast Test.**---The blast technique is based on a controlled detonation of explosives aimed at
3 generating long-duration cyclic shaking of the ground and testing the *in situ* soil liquefaction
4 potential, as recent experiments in New Zealand and the United States have shown (Wentz et al.,
5 2015; Finno et al., 2016). A blast test produces accelerations whose frequencies are significantly
6 higher than the real earthquakes, but the obtained ground velocity and displacement amplitudes are
7 similar to those generated by a strong earthquake. Sequential blasts can also induce multiple shear
8 strain cycles and generate a build-up of excess pore pressure, inducing liquefaction. *In situ*
9 geotechnical monitoring, laboratory investigations, and geophysical surveys are usually coupled
10 with the detonations to optimize their effectiveness (Gohl et al., 2009; Ashford et al, 2004; Rollins
11 et al, 2004) and to evaluate variations in soil parameters before and after liquefaction. The first
12 Italian blast experiment at the target site of Mirabello (Ferrara, Italy) was performed on May 2016
13 with various purposes, including the evaluation of the source layers of the blast-ejected sands and
14 the interpretation of the blast-induced liquefaction mechanism. The controlled blasting experiment
15 induced liquefaction in the trial field site because sand boils, mixes of sand and water that reach the
16 surface and commonly form sand volcanoes (e.g. Marcuson, 1978), were observed (Amoroso et al.,
17 2017). The blast research activities (Fig. 3) included an intensive geological, geotechnical, and
18 geophysical campaign before and after the implementation of two blast sequences. Pore-pressure
19 transducers and settlement profilometers were installed in order to measure, during and after the
20 blast test, the generation and subsequent dissipation of the pore-water pressure along with the
21 vertical deformations. Based on the subsoil model and liquefaction assessment provided by
22 Amoroso et al. (2017), the blast layout was designed considering two sequences of blast charges to
23 detonate separately. Further details of the blast test are reported in Passeri et al., (2018) and Pesci et
24 al. (2018).

25

1 **Cone-Penetration Test.**---Important stratigraphic information were deduced from the
2 comparative analysis of the cone-penetration tests (CPT) performed in the surroundings of the
3 trial area (Fig. 3) for the seismic microzonation studies of Mirabello municipality (CPTuB11,
4 CPTu019, CPTu13244; Geotema, 2014) and for the blast-test experiment (CPTu1, CPTu2,
5 CPTu3; Amoroso et al., 2017). The vertical variation trends of the penetration logs supported the
6 recognition of various fluvial depositional bodies, paleosols and peat levels.

7

8 **Sampling.**---A total of 35 samples were collected and analyzed for grain size and
9 composition. Samples are representative of blast-induced liquefied sands and of sands in the
10 subsurface (Tables 1 and 2, Figs. 3 and 4). Thirteen samples come from two cores (S1 and S3)
11 located in the test site that allowed to reconstruct the stratigraphy and sand horizons from the
12 surface down to 20 m (Fig. 4, Table 1). Sampling was particularly dense in the interval between
13 5 and 8 m, considered as the most critical liquefiable layer. Two samples come from the helical
14 system that anchored the CPT truck at 2 m depth (ANC1, ANC2). Eight samples are liquefied
15 sand induced by the blast test: three are representative of boils (C1, C2, C5) collected
16 immediately after the first detonation within the 5 m-radius blast ring (Fig. 5A), and five were
17 collected during and after the blast experiment around blast monitoring equipment (instrumented
18 micropile and profilometers). Sample SB2012 is a sand boil from the 2012 Emilia earthquake in
19 the studied area (Fig. 3A). Finally, eleven samples are from dikes that crosscut the shallow
20 subsurface in 2 trenches (2.0–2.5 m deep) dug in the test site named BH15 trench (8 m long) and
21 MPA4 trench (10 m long) (Fig. 3). Table 1 and Figs 5B, C report more detail on dike depth and
22 shape. Samples are from the center of the dikes. Exploratory trenches were excavated by Istituto
23 Nazionale di Geofisica e Vulcanologia (INGV, Rome, Italy) across the 2012 sand blows,
24 approximately 5 to 12 m from the blast center. Dikes are not observed to reach the surface in the
25 trench cross section. They likely represent sands liquefied during the 2012 earthquake and
26 possibly previous events (INGV, work in progress).

1

2 **Grain-Size Analyses.**---32 samples were analyzed using standard techniques: mechanical
 3 sieving for the sandy fraction and hydrometer analysis for fine-grained sediments. Sand samples
 4 consisting of a few hundreds of grams were washed with dilute H₂O₂ to remove organic matter
 5 and were air dried and mechanically sieved for granulometric and compositional analyses. Grain-
 6 size analyses are reported as the granulometric curve in Figure 6. Table 1 reports the fines
 7 content (FC) which represents percentage of particles finer than 0.075 mm. D₆₀, D₃₀, and D₁₀ are
 8 the diameters of the 60th, 30th, and 10th percentile of the granulometric curve. The coefficient
 9 of uniformity U is given by the ratio between D₆₀ and D₁₀, and the coefficient of curvature C is
 10 function of D₃₀, D₆₀, and D₁₀:

$$11 \quad C = \frac{D_{30}^2}{D_{10} \cdot D_{60}}$$

12 According to the Unified Soil Classification System (USCS, ASTM D2487-11 2011) the
 13 sands characterized by U > 6 and 1 < C < 3 are well-graded (or poorly sorted).

14 **Compositional Analyses.**--- Modal analyses were carried out on 32 samples of sands and on
 15 the sandy fraction of sandy silt. Point counting under transmitted-light microscopy was
 16 performed on the 0.125–0.250 mm fraction, according to the Gazzi-Dickinson method designed
 17 to minimize the dependence of the analysis on the grain size (Zuffa, 1985) and to support a
 18 comparison with previous compositional studies of the area (Lugli et al., 2004, 2007). Results of
 19 point counting (300 grains for each section) are presented in Table 2. For textural and
 20 provenance considerations we refer to studies of Weltje and Von Eynatten,(2004), Arribas and
 21 Tortosa (2003), and Garzanti et al. (2011); detrital carbonate lithics were identified according to
 22 Fontana (1991). Components not related to the original sand composition, such as authigenic
 23 carbonate concretions, were excluded from the final calculations.

24

25

RESULTS

1

2

Stratigraphy of the Blast Test Site

3

4 The shallow sedimentary succession (0–20 m) involved into the blast test was outlined by two
5 boreholes integrated with CPTu data (Fig. 4) and interpreted within the knowledge framework
6 deriving from a recent study on the geology of the area (Minarelli et al., 2016 and references
7 therein). We recognized different units from the older to the younger:

- 8 • unit A, from 20.5 m to 17 m below the surface. This is the deepest unit involved in the
9 blast-test investigation, and is formed by gray, medium- to coarse-grained sands. From the
10 integration of the blast test data with evidence of regional geology, we can assume that the unit
11 represents to the upper portion of the AES7 subsynthem, and accumulated into a braided-river
12 environment mainly during the Last Glacial Maximum (LGM).

13 Sediments above unit A represent the upper portion of AES8 and show a complex
14 sedimentary architecture. They can be subdivided into three superposed units:

- 15 • unit B1 (from 17 to 7.7 m). It consists of fine- to medium-grained sand intercalated with
16 poorly sorted silty sand. The lower portion, between 16 and 17 m, is coarser grained. At 13 m a
17 thin silty layer is present. Based on the detailed correlation of the CPTu and stratigraphic core
18 logs, the interval can be interpreted as a meander channel body. An organic-rich layer within the
19 unit in an adjacent area has been dated 4440 ± 40 yr BP by ^{14}C (Amorosi et al., 2008; Stefani et
20 al., 2018).

- 21 • unit B2 (from 7.7 to 5.9 m). It is formed by fine-grained sand and silty sand, with
22 subordinated intercalations of silt and, in the lower portion, argillaceous levels. The interval can
23 be interpreted as a fluvial levee complex, laterally grading into crevasse splays probably
24 accumulated between 4000 to 3000 years ago.

- 25 • unit B3 (from 5.9 to 0 m). Interfluvial depression and distal levee deposits made up of:
26 silt and clayey silt with subordinate coarser-grained sandy levels, interpretable as an interfluvial

1 depression (5.9–4.4 m); sandy silt layer with diagenetic carbonate nodules interpretable as a
2 palaeosol (4.4–4.1 m) associated with an emersion phase (Roman surface); dark-colored plastic
3 silt and clay (4.1–2.2 m) with an intercalation of organic-rich clay and peat (3.1–3.5 m) ($1080 \pm$
4 30 yr BP by ^{14}C ; Amoroso et al., 2017). Organic-rich levels are common also in the upper
5 portion of the unit, recording widespread interfluvial depression marshes; silty clay and silt (2.2–
6 0.7 m) referable to the distal portion of crevasses splays of the paleo-Reno River (post Medieval,
7 up to the 18th century); reworked materials by agricultural practises (0.7–0.0 m), containing
8 muddy sediments with brick fragments and extruded sands liquefied during the 2012 Emilia
9 earthquake.

10

11

Grain-Size Distribution

12

13 The analyzed samples range from almost pure sands to silt with a variable content of sand and
14 clay. Samples from cores (Fig. 6A) show a gradual increase in grain size from shallow to deepest
15 samples. In particular, samples from the upper portion (up to 6.5 m) are the finest, made up of
16 coarse silt and sandy silt with a clay content higher than 10%. Sands from 7 m to 18.5 m are
17 coarser grained and fit in a narrow field predominantly made up of fine- and medium-grained
18 sands; the amount of silt is 20 to 30%, and the percentage of clay is lower than 10%.

19 Induced liquefied sands are almost pure sands (Fig. 6B) with a very narrow range around
20 medium-grained sand. The amount of silt and clay is less than 10% (except LP2: 18%).

21 The dike samples are similar to blast-liquefied sands, but with a slightly higher percentage of
22 silt and clay (up to 24%); clay is less than 10%, except in sample S12NW (Fig.6B). Samples are
23 well sorted. We did not observe significant grain-size variation along dikes at different depths
24 (0.2 to 2.2 m; Table 1).

1 The fines content (FC, Table 1) in cores ranges between 32 and 78 % in samples from 5.9 to
2 7.7 m and is lower (28–39%) in deeper samples. A distinctly lower FC content (< 25%) is
3 recorded in the blast-induced liquefied sands (FC 5–22%) and in trench samples (FC 10–25%).
4 The coefficients of uniformity U and curvature C in samples from the boreholes show that the
5 silty sands are well-graded (i.e., they contain particles with a wide range of sizes). In contrast,
6 the blast-liquefied sands and dikes are well sorted.

7

8 *Composition of Sands*

9

10 Data from modal analyses are reported in Table 2 and in the ternary diagram Q+F
11 (quartz+feldspars), L (siliciclastic fine-grained lithics), C (carbonate lithics) of Figure 7. This
12 diagram, better than the traditional QFL, allows the compositional fields of fluvial sands in the
13 Po plain to be differentiated as discussed by Lugli et al. (2007).

14

15 **Fluvial Sands from Boreholes.**---Fluvial sandy sediments in the subsurface (sands and the
16 sandy fraction in sandy silt), both from cores S1 and S3, show varying compositions from
17 lithoarenitic to quartz-feldspar-rich (Fig. 7A). They are made up of quartz (single crystal and
18 polycrystalline) ranging from 36.6 to 55.6% of the bulk rock; the highest amounts are in the
19 deepest sands at 18.2 m. Feldspars, both plagioclase and K-feldspar, vary from 6.3 to 30.6%.
20 Siliciclastic lithic are fine-grained detrital rocks, siltstones and shales, and subordinate low-grade
21 metamorphic rocks. Lithics range from 8 to 27.7% with minor amounts in deeper sands. Shales
22 are well lithified, with an evident preferred orientation of clay minerals, and for these characters
23 they appear to have a detrital origin, derived from older pelitic successions. Volcanites, spilites,
24 and serpentinites are only minor components. Carbonate lithics range from 6.3 to 15.7% of the
25 bulk sand and are made up of micritic and sparitic limestones; spars of calcite are also included,

1 as they derive from the breakage of sparitic limestones and veins. Micas (muscovite and
2 chlorite), glauconitic grains, and Fe-oxides are minor components. Few diagenetic concretions
3 occur in some samples. Sands do not show any evidence of grain cementation, including the
4 deepest ones.

5 In the Q+F, L, C diagram (Fig. 7A), sands in the subsurface show a well-defined trend from
6 litharenitic to quartz–feldspar-rich compositions. In particular, sands at depth up to 7.7 m are, in
7 different proportion, more litharenitic, rich in fine-grained sedimentary lithics (siltstones and
8 shales) (Fig. 8A), while the deepest sands (samples from 8.5 to 18.5 m) are enriched in quartz
9 and feldspars and fit in a well defined field of arkosic composition (Figs. 8B, C).

10 *Provenance of Fluvial Sands:* based on type and abundance of lithic grains, which are mainly
11 sedimentary, both fine-grained siliciclastic and carbonate derived from the erosion of Apenninic
12 sedimentary units, shallow sands up to 7.7 m indicate a clear Apenninic provenance referable to
13 the paleo-Reno River. Deeper sands, richer in quartz and feldspars, with abundant micas and
14 very low siltstones and shales, show affinities with the Po River sands. The deepest sample of
15 sands at 18.2 m is the richest in quartz (Fig. 8C) and poorest in sedimentary lithics, and is linked
16 to the older unit A, deposited by the Po River during the Last Glacial Maximum.

17

18 **Blast-Induced Liquefied Sands.**---Liquefied sands from sand boils (Fig. 7B, 8D) are quite
19 homogeneous in composition. Total quartz ranges from 40.4 to 52.6%. Feldspars (both
20 plagioclase and K-feldspar) vary from 7 to 15.4%. Fine-grained siliciclastic lithics, made up of
21 siltstones, shales, and low-grade metamorphites, account for 15 to 25.8% of the whole sands.
22 Carbonate lithics, such as micritic and sparitic limestones, vary from 11.3 to 16.7%. Sands from
23 micropile (see Table 1) show similar compositions with more variations in quartz content.

24 Composition of liquefied sands overlap that of the shallow fluvial sands down to the depth of
25 7.7 m and clearly differ from layers deeper than 8 m, higher in quartz–feldspar content.

26

1 **Sand from Dikes in Trenches.** The sands filling the dikes in the trenches (Fig. 7C) show
2 relatively homogeneous compositions. Total quartz ranges from 33.4 to 48%, and feldspars from
3 10.7 to 20%. Siliciclastic lithics, largely low-grade metamorphics and shales, range from 12.6 to
4 23.8%. Carbonate lithics vary from 13.9 to 19.4%. We did not observe significant variations in
5 sands from single dikes at different depths. In the Q+ F,L,C diagram, sands from dikes plot in the
6 same field as shallow sands (up to 7.7 m).

7

8

9

DISCUSSION

10

11 The earthquake-simulation field experiment (blast test) carried out in Quaternary fluvial
12 sediments of the Emilia plain induced subsurface liquefaction and the formation of sand blows.
13 The grain size and composition of ejected sediments were compared with subsurface data from
14 boreholes and trenches. The main findings of the study are discussed with particular concern to
15 the recognition of the source layer and grain-size segregation mechanisms during liquefaction.

16

17

Stratigraphic Framework

18

19 Data from two boreholes and several cone-penetration tests supported the reconstruction of a
20 detailed stratigraphic framework of fluvial sediments in which the liquefiable layers are located
21 (Fig. 9). The deepest portion of the section (unit A) consists of Po River sands deposited in the
22 Late Pleistocene into braided channels during Last Glacial Maximum and late Glacial times
23 (LGM in Fig. 9). A thick sand body, interpreted as a Po River channel fill (unit B1) is identified
24 between 8 and 17 m. This is overlain by silty sands and silts from a paleo-Reno River levee body
25 (unit B2, 5.9–7.7 m), which accumulated approximately between 4000 to 3000 years ago. The

1 uppermost portion of the studied successions is largely formed by argillaceous sediments,
2 deposited in interfluvial swamp and distal levee areas of the paleo-Reno River in Medieval and
3 modern times (unit B3).

4

5

Source Layer Identification

6

7 The composition of sands liquefied by the blast test poses an important constraint in the
8 recognition of the source layer. Measurements of excess pore pressures and soil deformation
9 during the blast monitoring have detected a wide liquefiable layer that extended at least from 6 to
10 12 m depth (Amoroso et al., 2017). However, only silty sands of unit B2, between 5.9 and 7.7 m
11 deep, were ejected to the surface to form sand boils, as clearly deduced by petrographic analysis
12 (Fig. 7). In fact, the composition of sands from blows shows close similarity with shallow sands
13 of unit B2 at a depth from 5.9 to 7.7 m, while it clearly differs from deeper sands, which are
14 richer in quartz and feldspar and poorer in sedimentary lithic fragments. These data indicate that
15 the ejected layer largely corresponds to the fluvial Apenninic deposits of the paleo-Reno River,
16 while the underlying sands referable to a paleochannel of the Po River (unit B1 and A) were not
17 involved.

18 Our data also show that the composition of blast-induced sand boils overlap that of dikes in
19 trenches of the blast area. As already reported by Amoroso et al. (2017), dikes are fractures
20 infilled by sands injected upward during the 2012 earthquake or older events. This indicates that
21 sand layers liquefied by seismic events are the same as induced by the blast test.

22 Results from the blast test fit well with data obtained from the study of the sands ejected in
23 the nearby area of San Carlo during the M_L 5.9 earthquake (Fontana et al., 2015). Even in this
24 case, sand composition and fabric indicate that liquefaction processes mainly affected sand
25 layers at relatively shallow depth (6.8–7.5 m) characterized by litharenitic composition, and did
26 not affect deeper sands, Holocene to Pleistocene in age, with a quartz–feldspar-rich composition.

1 In all these cases, the liquefied sands share a litharenitic composition, with abundant lithic
2 fragments of micritic limestones, shales, and siltstones, usually rounded in shape, rather than
3 sands rich in quartz and feldspars angular in shape. It is reported in the literature that the
4 presence of rounded grains is one factor that can increase the liquefaction susceptibility (Kramer,
5 1996), but very little data are available on petrography of liquefied sands and injectites (Ross et
6 al., 2014). It could be that specific compositions favor liquefaction rather than others, but further
7 studies are necessary to validate this factor.

8 9 *Grain-Size Characteristics and Liquefaction Susceptibility*

10
11 The grain-size characteristics of the examined sands are compared to data reported in the
12 literature for sands ejected during earthquakes. Several papers (Kishida, 1970; Tokimatsu and
13 Yoshimi, 1983; Figueroa et al., 1995) report that mainly clean sand with a low natural clay
14 content are susceptible to liquefaction, and report a cut-off for liquefaction susceptibility at a
15 clay content of about 10–15%. The liquefaction susceptibility of fine-grained sediments has been
16 debated over the last 20 years (e.g., Andrew and Martin, 2000; Idriss and Boulanger, 2008; Bray
17 et al., 2014; Boncio et al., 2018): fine-grained sediments were considered incapable of generating
18 the high pore pressures commonly associated with liquefaction (Kramer 1996). Only a few
19 papers (Ishihara, 1984; Chang et al, 2011) observed liquefaction of non-plastic silts, indicating
20 that plasticity characteristics rather than grain size alone influence the liquefaction susceptibility
21 of fine-grained soils. Non-plastic and cohesionless coarse silts with bulky particle shape are fully
22 susceptible to liquefaction, while finer silts with flaky or plate-like particles generally exhibit
23 sufficient cohesion to inhibit liquefaction (Ishihara 1993).

24 Since our study takes into consideration not only the characteristics of the sands that reach the
25 surface but also those of the buried source layer, the effects of particle size in the liquefaction
26 processes can be better outlined. Liquefied sands that reached the surface are well-sorted

1 medium-grained sands with silt and clay content less than 10%; they fall within the expected
2 parameters for liquefaction. However, when comparing liquefied sands with their source layer at
3 5.9–7.7 m depth (Fig. 6), we observe that “source” sands have a higher amount of fine-grained
4 particles (silt and clay > 30%; clay < 15%). This has two interesting implications.

5 Firstly, the source beds can contain higher amounts of silt than reported in many previous
6 liquefaction studies, indicating that also coarse silts and silty sands are fully susceptible to
7 liquefaction. This aspect has to be considered while estimating the liquefaction potential hazard.
8 Poorly sorted sands and finer-grained sediments are more susceptible to liquefaction phenomena
9 than previously thought.

10 Secondly, we observe that there is a selective loss of fines in the dikes and sand volcanoes
11 relative to the source beds, indicating that the liquefaction process appears to be able to select the
12 diameters of the grains that reach the ground surface. This effect is well observed in the blast-
13 induced liquefaction and in 2012 sand boil ejected in the same area (sample SB 2012, Fig. 6B)
14 and to a lesser extent in the trench dikes (yellow curves in Fig. 6B).

15

16 *Grain-Size Segregation during Liquefaction*

17

18 Studies and experiments on liquefaction and fluidization of silty sand sediments, as occurs in
19 dikes and sand volcanoes, suggest that sorting may occur within the source bed and dikes, and
20 further separation occurs as the material is extruded (e.g., Diggs, 2007; Ross et al., 2011). As
21 pore pressure builds, finer-grained material may be moved into the surrounding sediment,
22 forming an infiltration horizon and the slightly cleaner sediment can then break through this
23 infiltration horizon and be injected upwards (Ross et al., 2011). Segregation can also occur in the
24 injected dikes, with Ross et al. (2011) showing that fines can line the pipe walls as water flows
25 radially out of the pipe due to the flow velocity gradient between the pipe and the ambient
26 velocity in the surrounding sediment. This pipe-lining phenomenon has been observed elsewhere

1 (Mount, 1993, Diggs, 2007, Kazerouni et al., 2011, Ross et al., 2014). Once the fluidized flow
2 hits the surface then further segregation can occur. Ross et al. (2013) show for subaqueous sand
3 volcanoes that clay and grain size decrease with increasing distance from the vent, which they
4 interpret as a result of settling of the coarsest particles close to the vent, and preferential transport
5 of the clay within the currents. Such processes also occur in subaerial systems: Quigley et al.,
6 (2013) show silt drapes on the top of sand volcanoes between liquefaction-inducing earthquakes,
7 which they interpret as drapes from suspended sediment as ejected ground-water drained
8 following the liquefaction event. The clay, and potentially some of the finer silts, become part of
9 a pseudofluid (Di Felice, 2010; Ross et al., 2014) and travels with the fluid phase whilst the
10 larger particles are deposited from this suspension. Such fine-rich fluids can be seen in videos of
11 earthquake-induced eruptions of sand volcanoes, such as those in Christchurch, New Zealand,
12 described by Quigley et al. (2013). Pulse flows are hypothesized in dikes and sand blows in
13 liquefaction sites due to the 2012 Emilia earthquake described by Fontana et al (2015) and
14 Rodríguez-Pascua et al. (2015). The sedimentary features (inverse and normal grading, vertical
15 and concave lamination) suggest that fractures were rhythmically injected and filled by a slurry
16 of sand and mud during the compression pulses, and emptied by the rushing of the slurry back
17 down deep into the fractures during the extension peak, forming laminated structures in sand
18 volcanoes on the top of the fractures (millimeter- to centimeter-thick alternating graded laminae
19 of sand and mud).

20 In interpreting results from our study (Fig. 10), we cannot exclude differences between
21 shaking generated by the blast test versus earthquake. In fact, a blast test produces accelerations
22 whose frequencies are significantly higher than real earthquakes, but the obtained ground
23 velocity and displacement amplitudes should be similar to those generated by a strong
24 earthquake (Amoroso et al., 2017). Data from this study confirm that some sorting occurs within
25 dikes, and further sorting occurs as the material is extruded (both in blast-liquefied sands and in
26 2012 earthquake sand boil), probably following the generated excess pore-water pressure. This

1 may have caused the segregation and dispersion of the fine silt–clay content, producing highly
2 sorted sand boils. Instead it seems that the selective mechanism due to ejection of liquefied sands
3 has not influenced the sand composition (see also Fontana et al., 2015), and that disintegration or
4 erosion of the most erodible grains due to the abrasive flow of sand grains is almost negligible.

6 CONCLUSIONS

7
8 • Study of the sands ejected during the blast test in the Mirabello area (Po plain), and
9 comparison of their texture and composition with those of buried fluvial sediments as deep as 20
10 m supported a reliable source-layers identification.

11 • Ejected sands show a litharenitic composition that largely overlap that of the shallow
12 Apenninic sands down to the depth of 5.9–7.7 m. These sands clearly differ from deeper sands,
13 enriched in quartz and feldspars, largely referred to paleochannels of the Po River.

14 • Similarly the sands from the dikes show a composition compatible with that of the
15 shallow sands of Apenninic affinity, suggesting that liquefied layer during the 2012 seismic
16 crisis are the same as that induced by blast test.

17 • The study indicates that silty sands and silts characterized by relatively high fines content
18 (FC 32–76%) can also liquefy, differently from what reported in most of the literature.

19 • The liquefaction process appears to be able to select the diameters of the grains which
20 reach the ground surface. Some sorting occurs within injected dikes, probably due to pulse flows,
21 and further segregation occurs as the material is extruded following the generated excess pore-
22 water pressure. This may have caused the dispersion of the fine silt–clay content, producing
23 highly sorted sand boils.

24 • The study indicates that we have a significant tool for a better understanding of
25 earthquake-induced liquefaction mechanisms, using textural and petrographic parameters to

1 correlate ejected sands with their buried source beds. This is pivotal for the recognition of
2 potential areas prone to hazardous sand liquefaction phenomena.

3

4

5

ACKNOWLEDGMENTS

6

7 The study was mainly funded by FIRB-Abruzzo project (<http://progettoabruzzo.rm.ingv.it/it>).

8 Special thanks to Prof. Kyle M. Rollins for contributing to the realization of the blast-test

9 experiment in terms of personnel and technical equipment. We are indebted to David Hodgson,

10 Jeff Peakall, and Geraint Owen for the accurate revision and relevant suggestions that greatly

11 improved the manuscript. Many thanks to Simona Marchetti Dori for the support in grain-size

12 analyses and to Paolo Marco De Martini, Francesca Cinti, Alessandra Smedile, and Riccardo

13 Civico (INGV, Rome, Italy) for opening the two trenches in the trial site of Mirabello.

14

15

16

REFERENCES

17

18 Amorosi, A., Pavesi, M., Ricci Lucchi, M., Sarti, G., and Piccin, A., 2008, Climatic signature of

19 cyclic fluvial architecture from the Quaternary of the central Po Plain, Italy: *Sedimentary*

20 *Geology*, v. 209, p. 58–68.

21 Amorosi, A., Bruno, L., Facciorusso, J., Piccin, A., and Sammartino, I., 2016, Stratigraphic control

22 on earthquake-induced liquefaction: A case study from the Central Po Plain (Italy): *Sedimentary*

23 *Geology*, v. 345, p. 42–53.

24 Amoroso, S., Milana, G., Rollins K.M., Comina, C., Minarelli, L., Manuel, M.R., Monaco, P.,

25 Franceschini, M., Anzidei, M., Lusvardi, C., Cantore, L., Carpena, A., Casadei, S., Cinti, F.R.,

26 Civico, R., Cox, B.R., De Martini, P.M., Di Giulio, G., Di Naccio, D., Di Stefano, G.,

- 1 Facciorusso, J., Famiani, D., Fiorelli, F., Fontana, D., Foti, S., Madiari, C., Marangoni, V.,
2 Marchetti, D., Marchetti, S.L., Martelli, L., Mariotti, M., Muscolino, E., Pancaldi, D., Pantosti,
3 D., Passeri, F., Pesci, A., Romeo, G., Sapia, V., Smedile, A., Stefani, M., Tarabusi, G., Teza, G.,
4 Vassallo, M. and Villani, F., 2017, The first Italian blast-induced liquefaction test (Mirabello,
5 Emilia-Romagna, Italy): description of the experiment and preliminary results: *Annals of*
6 *Geophysics*, v. 60(5), no. S0556.
- 7 Andrew, D.C.A., and Martin, G.R., 2000, Criteria for liquefaction of silty soils, in 12th world
8 conference on earthquake engineering: Auckland, New Zealand, Proceedings, Paper 0312.
- 9 Argnani, A., Fontana, D., Stefani, C., and Zuffa, G.G., 2006, Palaeogeography of the Upper
10 Cretaceous-Eocene carbonate turbidites of the Northern Apennines from provenance studies:
11 *Geological Society of London Journal*, v. 262, p. 259–275,
- 12 Arribas, J., and Tortosa, A., 2003, Detrital modes in sedimenticlastic sands from first-order streams
13 of the Iberian Range, Spain: The potential for sand generation of different sedimentary rocks:
14 *Sedimentary Geology*, v. 159, p. 275–303.
- 15 Ashford, S., Rollins, K.M., and Lane, J., 2004, Blast-induced liquefaction for full-scale foundation
16 testing: *Journal of Geotechnical and Geoenvironmental Engineering*, v. 130(8), p. 798–806.
- 17 ASTM D2487-11, 2011, Standard Practice for Classification of Soils for Engineering Purposes
18 (Unified Soil Classification System).
- 19 Boccaletti, M., Bonini, M., Corti, G., Gasperini, P., Martelli, L., Piccardi, L., Severi, P., and
20 Vannucci, G., 2004, Seismotectonic map of the Emilia-Romagna Region: Regione Emilia-
21 Romagna –CNR, SELCA, Firenze.
- 22 Boncio, P., Amoroso, S., Vessia, G., Francescone, M., Nardone, M., Monaco, P., Famiani, D., Di
23 Naccio, D., Mercuri, A., Manuel, M.R., Galadini, F., and Milana, G., 2018, Evaluation of
24 liquefaction potential in an intermountain Quaternary lacustrine basin (Fucino basin, central
25 Italy): *Bulletin of Earthquake Engineering*, v. 16(1), p. 91-111.

- 1 Bray, J., and Sancio R.B., 2006, Assessment of the liquefaction susceptibility of fine-grained soils:
2 Journal of Geotechnical and Geoenvironmental Engineering, v. 132(9), p. 1165–1177.
- 3 Bray, J., Cubrinovski, M., Zupan, J., and Taylor, M., 2014, Liquefaction effects on buildings in the
4 central business district of Christchurch: Earthq Spectra, v. 30(1), p. 85–109.
- 5 Caputo, R., and Papathanasiou, G., 2012, Ground failure and liquefaction phenomena triggered by
6 the 20 May, 2012 Emilia-Romagna (Northern Italy) earthquake: case study of Sant'Agostino–San
7 Carlo–Mirabello zone: Natural Hazards and Earth System Sciences, v. 12(11), p. 3177–3180.
- 8 Carminati, E., Doglioni, C., and Scrocca D., 2005, Magnitude and causes of long-term subsidence
9 of the Po Plain and Venetian region, *in* Fletcher, C.A., and Spencer, T., with Da Mosto, J., and
10 Campostrini, P., eds., *Flooding and Environmental Challenges for Venice and its Lagoon: State
11 of Knowledge*: Cambridge, UK, Cambridge University Press, p. 21-28.
- 12 Chang, W.J., Ni, S.H., Huang, A.B., Huang, Y.H., and Yang, Y.Z., 2011, Geotechnical
13 reconnaissance and liquefaction analyses of a liquefaction site with silty fine sand in Southern
14 Taiwan: Engineering Geology, v. 123, p. 235–245.
- 15 Chen, L., Hou, L., Cao, Z., Yuan, X., Sun, R., Wang, W., Mang, F., Chen, H. and Dong, L., 2008,
16 Liquefaction investigation of Wenchuan earthquake, *in* 14th World Conference on Earthquake
17 Engineering: Beijing, China, Proceedings, S31–049.
- 18 Cobain, S.L., Hodgson, D.M., Peakall, J., and Shiers., M.N., 2017, An integrated model of clastic
19 injectites and basin floor lobe complexes: Implications for stratigraphic trap plays: Basin
20 Research, v. 29, p. 816–835.
- 21 Di Felice, R., 2010, Liquid–solid suspension theory with reference to possible applications in
22 geology: Basin Research, v. 22, p. 591–602.
- 23 Diggs, T.N., 2007, An outcrop study of clastic injection structures in the Carboniferous Tesnus
24 Formation, Marathon Basin, Trans-Pecos Texas, *in*: Hurst A. and J. Cartwright J. eds., *Sand
25 Injectites: Implications for Hydrocarbon Exploration and Production* : American Association of
26 Petroleum Geologists Memoir, v. 87, p. 37–48.

- 1 Emergeo Working Group, 2013, Liquefaction phenomena associated with the Emilia earthquake
2 sequence of May–June 2012 (Northern Italy): *Natural Hazards and Earth System Sciences*, v.
3 13(4), p. 935–947.
- 4 Figueroa, J.L., Saada, A.S., and Liang, L., 1995, Effect of the grain size on the energy per unit
5 volume at the onset of liquefaction, *in* 3rd International Conference on Recent Advances in
6 Geotechnical Earthquake Engineering and Soil Dynamics: St. Louis, Missouri, Proceedings, v. 1,
7 p. 197–202.
- 8 Finno, R.J, Gallant, A.P. and Sabatini, P.J., 2016, Evaluating ground improvement after blast
9 densification at the oakridge landfill: *Journal of Geotechnical and Geoenvironmental*
10 *Engineering*, v. 142 (1), p. 1–13.
- 11 Fioravante, V., Giretti, D., Abate, G., Aversa, S., Boldini, D., Capilleri, P., Cavallaro, A.,
12 Chamlagain, D., Crespellani, T., Dezi, F., Facciorusso, J., Ghinelli, A., Grasso, S., Lanzo, G.,
13 Madaia, C., Massimino, M.R., Maugeri, M., Pagliaroli, A., Ranieri, C., Tropeano, G., Santucci De
14 Magistris, F., Sica, S., Silvestri, F. and Vannucchi, G., 2013, Earthquake geotechnical
15 engineering aspects: the 2012 Emilia-Romagna earthquake (Italy), *in* 7th International
16 Conference on Case Histories in Geotechnical Engineering: Chicago, Illinois, Proceedings, p. 1–
17 34.
- 18 Fontana, D., 1991, Detrital carbonate grains as provenance indicators in the Upper Cretaceous
19 Pietraforte Formation (northern Apennines): *Sedimentology*, v. 38, p. 1085–1095.
- 20 Fontana, D., Lugli, S., Marchetti Dori, S., Caputo, R., and Stefani, M., 2015, Sedimentology and
21 composition of sands injected during the seismic crisis of May 2012 (Emilia, Italy): clues for
22 source layer identification and liquefaction regime: *Sedimentary Geology*, v. 325, p. 158–167.
- 23 Garzanti, E., Vezzoli, G., and Andò, S., 2011, Paleogeographic and paleodrainage changes during
24 Pleistocene glaciations (Po Plain, Northern Italy): *Earth-Science Reviews*, v. 105 (1-2), p. 25–48.

- 1 Geotema, 2014, Microzonazione sismica livello 2 con locali approfondimenti di livello 3, del
2 Comune di Mirabello (FE), Regione Emilia-Romagna: Relazione illustrativa e 7 tavv. (in Italian).
3 http://www.comune.mirabello.fe.it/files/00036/relazione_ms_mirabello.pdf
- 4 Ghielmi, M., Minervini, M., Nini, C., Rogledi, S., and Rossi, M., 2013, Late Miocene e Middle
5 Pleistocene sequences in the Po Plain–Northern Adriatic Sea (Italy): the stratigraphic record of
6 modification phases affecting a complex foreland basin: *Marine and Petroleum Geology*, v. 42, p.
7 50–81.
- 8 Giona Bucci, M., Almond, P., Villamor, P., Ries, W., Smith, C., and Tuttle, M., 2017, When the
9 earth blisters: Exploring recurrent liquefaction features in the coastal system of Christchurch,
10 New Zealand: *Terra Nova*, v. 29(3), p. 162-172.
- 11 Gohl, W.B., Martin, T., and Elliott, R.J., 2009, Explosive compaction of granular soils and in situ
12 liquefaction testing using sequential detonation of explosives, *in* International Symposium on
13 Ground Improvement Technologies and Case Histories: Singapore, Geotechnical Society of
14 Singapore, Proceedings, p. 199–207.
- 15 Hurst, A., Scott A., and Vigorito M., 2011, Physical characteristics of sand injectites: *Earth-Science*
16 *Reviews*, v. 106, p. 215–246.
- 17 Kazerouni, A.M., Friis, H., Svendsen, J.B., and Weibel, R., 2011, Heavy mineral sorting in
18 downwards injected Palaeocene sandstone, Siri Canyon, Danish North Sea: *Sedimentary*
19 *Geology*, v. 236, p. 279–285.
- 20 Kishida, H., 1970, Characteristics of Liquefaction of Level Sandy Ground During the Tokachioki
21 Earthquake: *Soils and Foundations*, v. 10(2), p. 103–111.
- 22 Kramer, S.L., 1996, *Geotechnical Earthquake Engineering: Upper Saddle River, New Jersey,*
23 *Prentice Hall, Inc., 653 p.*
- 24 Krinitzsky, E.L., Chang, F.K., and Nuttli, O.W., 1988, Magnitude-related earthquake ground
25 motions: *Association of Engineering Geologists Bulletin*, v. 25(4), p. 399–423.

- 1 Idriss, I.M., and Boulanger, R.W., 2008, Soil Liquefaction during Earthquakes: Earthquake
2 Engineering Research Institute, Monograph MNO-12, 237 p.
- 3 Ishihara, K., 1984, Post-earthquake failure of a tailings dam due to liquefaction of the pond deposit:
4 International Conference on Case Histories in Geotechnical Engineering: St. Louis, Missouri,
5 Proceedings, v. 3, p. 1129-1143.
- 6 Ishihara, K., 1993, Liquefaction and flow failure during earthquakes: *Geotechnique*, v. 43(3), p.
7 351-415.
- 8 Lugli, S., Marchetti Dori, S., Fontana, D., and Panini, F., 2004, Composition of sands in cores along
9 the high-speed rail (TAV): Preliminary indications on the sedimentary evolution of the Modena
10 plain: *Alpine and Mediterranean Quaternary*, v. 17(1-2), p. 379-389.
- 11 Lugli, S., Marchetti Dori, S., and Fontana, D., 2007, Alluvial sand composition as a tool to unravel
12 the Late Quaternary sedimentation of the Modena plain, northern Italy, *in* Arribas, J., Critelli, S.,
13 and Johnsson, M.J., eds., *Sedimentary Provenance and Petrogenesis: Perspectives from*
14 *Petrography and Geochemistry: Geological Society of America, Special Paper, 420, p. 57–72.*
- 15 Marcuson, W.F., 1978, Definition of terms related to liquefaction: American Society of Civil
16 Engineers, Proceedings, *Journal of the Geotechnical Engineering Division*, v. 104(9), p. 1197-
17 1200.
- 18 Mariotti, G., and Doglioni, C., 2000, The dip of the foreland monocline in the Alps and Apennines:
19 *Earth and Planetary Science Letters*, v. 181, p. 191–202.
- 20 Minarelli, L., Amoroso, S., Tarabusi, G., Stefani, M., and Pulelli, G., 2016, Down-hole geophysical
21 characterization of middle–upper Quaternary sequences in the Apennine Foredeep, Mirabello,
22 Italy: *Annals of Geophysics*, v. 59(5), no. S0543.
- 23 Mitchell, J.K., and Soga, K., 2005, *Fundamentals of Soil Behavior: Third Edition*, Hoboken, New
24 Jersey, John Wiley and Sons, 558 p.
- 25 Mount, J.F., 1993, Formation of fluidization pipes during liquefaction: examples from the Uratanna
26 Formation (Lower Cambrian), South Australia: *Sedimentology*, v. 40, p. 1027–1037.

- 1 Nichols, R.J., Sparks, R.S.J., and Wilson, C.J.N., 1994, Experimental studies of the fluidization of
2 layered sediments and the formation of fluid escape structures: *Sedimentology*, v. 41, p. 233–253.
- 3 Owen, G. and Moretti, M., 2011, Identifying triggers for liquefaction-induced soft-sediment
4 deformation in sands: *Sedimentary Geology*, v. 235(3-4), p. 141–147.
- 5 Passeri, F., Comina, C., Marangoni, V., Foti, S., And Amoroso S., 2018, Geophysical tests to
6 monitor blast-induced liquefaction, the Mirabello (NE, Italy) test site: *Journal of Environmental
7 and Engineering Geophysics*, v. 23(3), p. 319–333,
- 8 Pesci, A., Amoroso, S., Teza, G., and Minarelli, L., 2018, Characterisation of soil deformation due
9 to blast-induced liquefaction by UAV-based photogrammetry and terrestrial laser scanning:
10 *International Journal of Remote Sensing*, 20 p., doi: 10.1080/01431161.2018.1484960.
- 11 Quigley, M., Bastin, S., and Bradley, B., 2013, Recurrent liquefaction in Christchurch, New
12 Zealand during the Canterbury earthquake sequence: *Geology*, v. 41(4), p. 419–422.
- 13 Ricci Lucchi F., 1986, The Oligocene to Recent foreland basins of the Northern Apennines: *in*
14 Allen P.A., and Homewood P., eds., *Foreland Basin*, International Association of
15 Sedimentologists, Special Publication 8, p. 105–139.
- 16 Rodríguez-Pascua, M.A., Pablo G. Silva, P.G., Perez-Lopez, R., Giner-Robles, J.L., Martín-
17 Gonzalez, F., and Del Moral, B., 2015, Polygenetic sand volcanoes: On the features of
18 liquefaction processes generated by a single event (2012 Emilia Romagna 5.9 M_w earthquake
19 Italy): *Quaternary International*, v. 357, p. 329–335.
- 20 Rollins, K.M., Lane, J.D., Nicholson, P.G., and Rollins, R.E., 2004, Liquefaction hazard assessment
21 using controlled blasting techniques, *in* 11th International Conference on Soil Dynamics and
22 Earthquake Engineering: Berkeley, California, Proceedings, v. 2, p. 630–637.
- 23 Ross, J.A., Peakall, J., and Keevil, G.M., 2011, An integrated model of extrusive sand injectites in
24 cohesionless sediments: *Sedimentology*, v. 58, p. 1693–1715.
- 25 Ross, J.A., Peakall, J., and Keevil, G.M., 2013, Sub-aqueous sand extrusion dynamics: the
26 *Geological Society of London Journal*, v. 170, p. 593–602.

- 1 Ross, J.A., Peakall, J., and Keevil, G.M., 2014, Facies and flow regimes of sandstone-hosted
2 columnar intrusions: insights from the pipes of Kodachrome Basin State Park: *Sedimentology*, v.
3 61, p.1764–1792.
- 4 Stefani, M., Minarelli, L., Fontana, A. and Hajdas, I., 2018, Regional deformation of Late
5 Quaternary fluvial sediments in the Apennines foreland basin (Emilia, Italy): *International*
6 *Journal of Earth Sciences*, 15 p., doi:10.1007/s00531-018-1606-x.
- 7 Tokimatsu, K., and Yoshimi, Y., 1983, Empirical correlation of soil liquefaction based on SPT N-
8 value and fines content: *Soils and Foundations*, v. 23(4), p. 56–74.
- 9 Weltje, G.J., and Von Eynatten, H., 2004, Quantitative provenance analysis of Sediments: Review
10 and outlook: *Sedimentary Geology*, v. 171, p. 1–11.
- 11 Wentz, F.J., van Ballegooy, S., Rollins, K.M., Ashford, S.A., and Olsen, M.J., 2015, Large scale
12 testing of shallow ground improvements using blast-induced liquefaction, *in* 6th International
13 Conference on Earthquake Geotechnical Engineering: Christchurch, New Zealand, Proceedings.
- 14 Youd, T.L., and Perkins, D.M., 1978, Mapping liquefaction induced ground failure potential:
15 American Society of Civil Engineers, Proceedings, *Journal of the Geotechnical Engineering*
16 *Division*, v. 104(4), p. 443–446.
- 17 Zuffa, G.G., 1985, Optical analyses of arenites: influence of methodology on compositional results,
18 *in* Zuffa, G., ed., *Provenance of Arenites*: Dordrecht, Netherlands, D. Reidel, NATO Advanced
19 Study Institute, v. 148, p. 165–189.

FIGURE CAPTIONS

1
2
3
4
5
6
7
8
9
10
11
12
13
14
15
16
17
18
19
20
21
22
23
24
25
26

Fig. 1.---Map of the Emilia alluvial plain showing the blast test site of Mirabello. The area was affected by the 2012 earthquakes (two major epicenters are located) that generated numerous sand boils (red dots) (data from Emergeo Working Group, 2013; Caputo and Papathanasiou, 2012). At the end of 18th century the course of the Reno River was artificially forced to reach the Adriatic sea. The studied site is located just northeast of the diversion point, along the buried paleochannel.

Fig. 2.---Simplified stratigraphic section of the Ferrara alluvial plain (modified from Geotema, 2014). The deepest succession (AES7) is dominated by sands accumulated during the Last Glacial Maximum (LGM) (late Pleistocene). The overlying successions (AES8) is made up of Holocene fluvial channel and levee sands and silts alternating with silt and clay recording wide continental swamps. The upper portion of the AES8 is dominated by the large sand body of the Reno River flanked by its levee and interfluvial deposits

Fig. 3.---A) Location map of the trial Mirabello blast test site showing the CPTu tests and 2012 sand boils (modified from Amoroso et al., 2017). B) Detail of blast investigations with location of blast-induced sand boils and trenches.

Fig. 4.---Stratigraphy of the two cores S1 and S2, coupled with cone-tip resistance profile. Four units are distinguished: A, B1, B2, and B3. Samples examined in this work are reported along the sections.

Fig 5.---A) Blast-induced sand boils (C1) after the first detonation. Sample C1 is 15 cm distant from the center; the sand sheet is 7 cm thick. B) Sketch of sand dikes in the BH15 trench and location of

1 sample S2 NW (1.4 m of depth from the topographic surface). C) Detail of sand dikes (see sample
2 S2 for comparison). The width of dikes is around 5 cm

3 Fig 6.---Cumulative grain-size distributions of examined samples. A) Curves of samples from
4 cores S1 and S2 plus anchor of CPTu2 piezocone test. B) Granulometric curves of induced
5 liquefied sands (C1, C2, C3, LP1, LP2, LPS, and MPA1), of the SB2012 sand boil and of dikes.

6

7 Fig 7.--- Q+F, L, C diagram showing the composition of examined sands. A) Sands from cores.
8 B) liquefied sands from the blast test. C) Sands from dikes in trenches. Q, total quartz; F, total
9 feldspars; L, siliciclastic lithic fragments; C, carbonate lithic fragments. Numbers in core
10 samples refer to depth.

11

12 Fig. 8.---Photomicrographs of the examined sands. A) Sand from core S1 at depth of 6.2 m, with
13 abundant sedimentary lithic fragments indicating an Apenninic provenance (Reno River). B) Sand
14 from core S1 at depth of 9.4 m rich in quartz and feldspars referable to the paleo Po River. C) Sands
15 from the deepest horizon (S1 18.2) referable to the older Po River sands accumulated during the
16 Last Glacial Maximum. D) Liquefied sands from sand boil C5. Transmitted light, crossed polars. Q,
17 quartz; Qpx, polycrystalline quartz; F, feldspar; Sh, shale; St, siltstone; C, limestone; Cs, calcite
18 spar, M, micas.

19

20 Fig. 9.--- Stratigraphic scheme of the successions involved in the blast test. Source layer for
21 the ejected liquefied sands is the unit B2 at 5.7–7.7 m depth, represented by levee silty sands and
22 silts of the paleo-Reno River. Underlying sands of unit B1 were not involved in the ejection.

23

24 Fig. 10.---Sketch of the stratigraphy and various potential source layers in fluvial sediments of
25 the Emilia alluvial plain, with compositional and grain-size characteristics. Selective

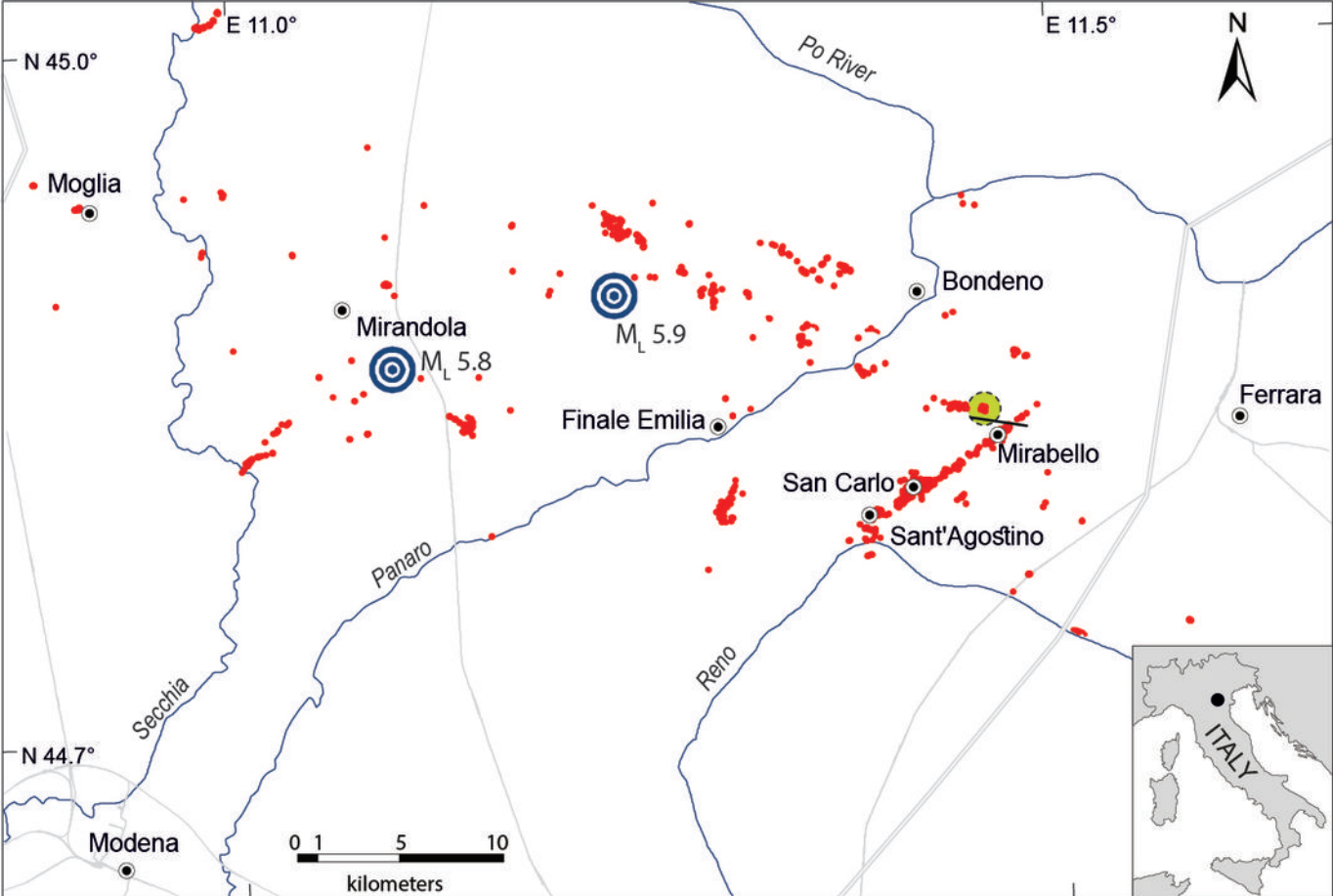
1 mechanisms during liquefaction, that might have caused grain-size segregation within dikes and
2 as the material is extruded, are shown. Symbols refer to Fig. 9.

3

4 Table 1.--- Granulometric properties of the analyzed samples: FC is the fines content; D_{60} , D_{30} ,
5 and D_{10} are the diameters of the 60th, 30th, and 10th percentile of the granulometric curve; U is the
6 coefficient of uniformity; C is the coefficient of curvature.

7

8 Table 2.--- Compositional modal analyses of examined sands (r.f.: rock fragment). Composition
9 is determined based on transmitted-light spectroscopy of the 125-250 micrometer fraction.



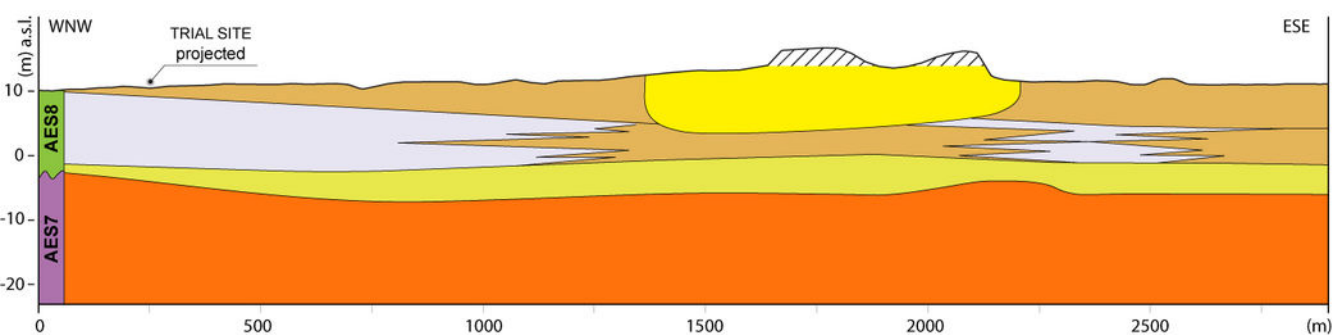
● urban center







● sand boils

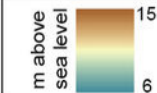
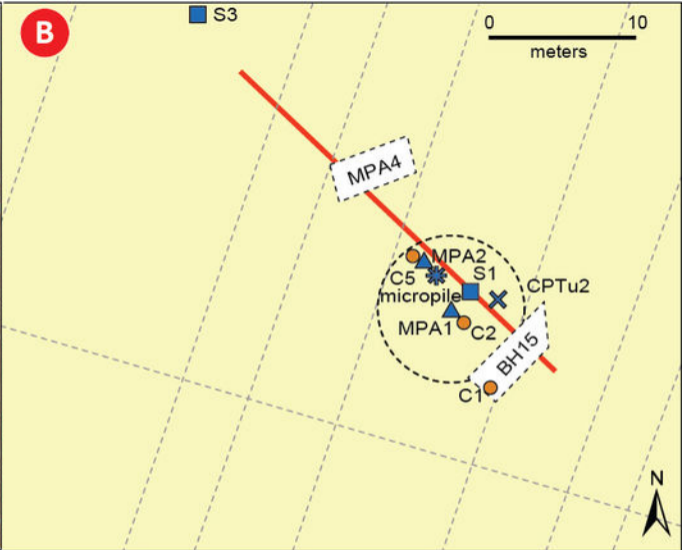
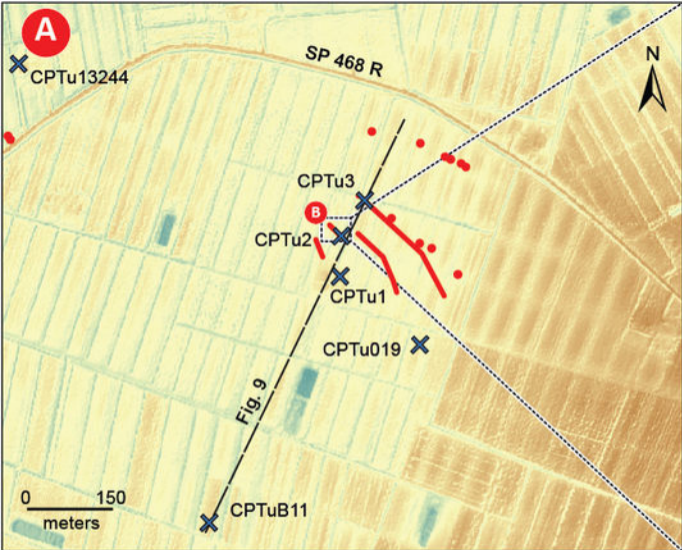
● 2012 major earthquake epicentre

● trial blast site

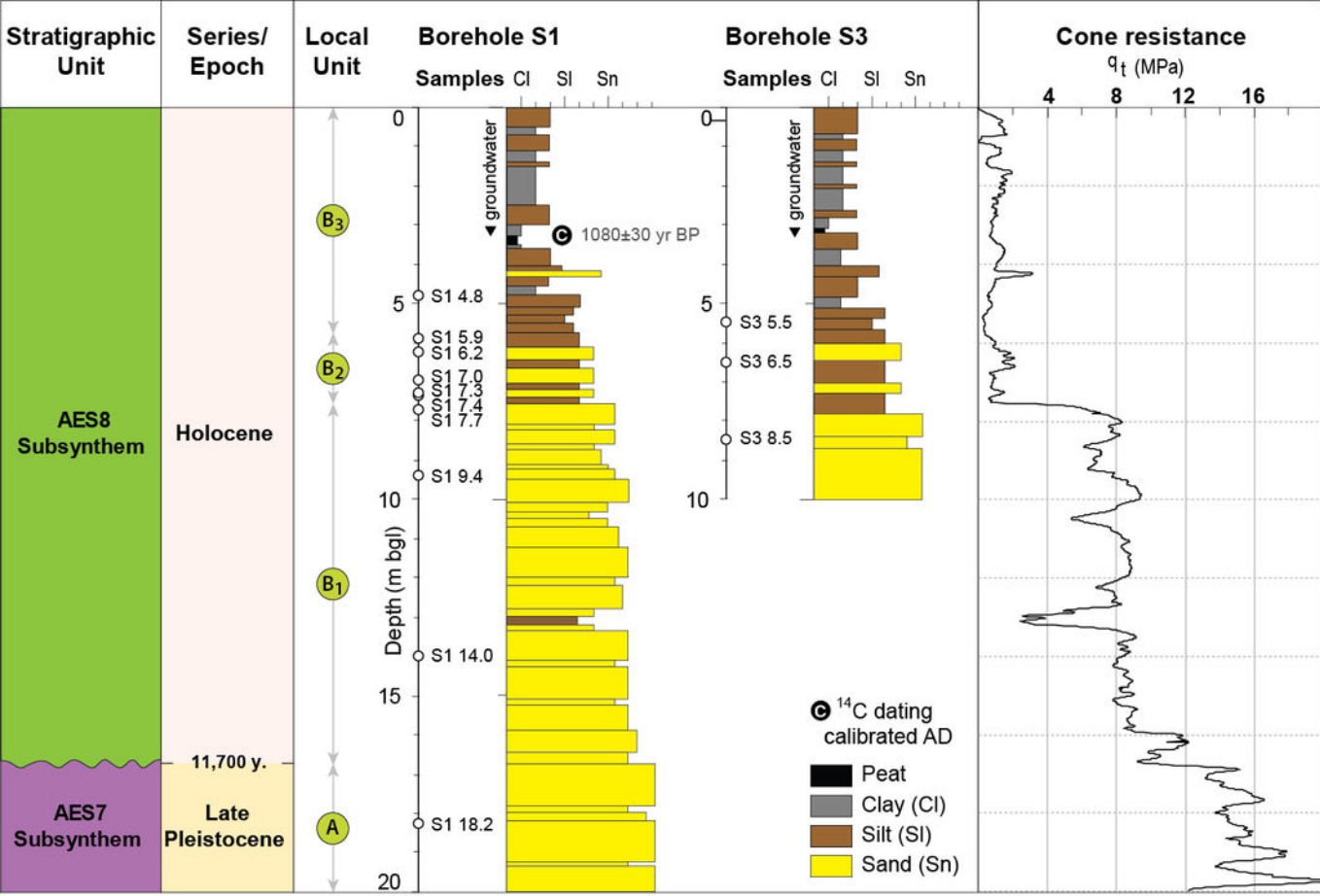
— trace of subsurface profile

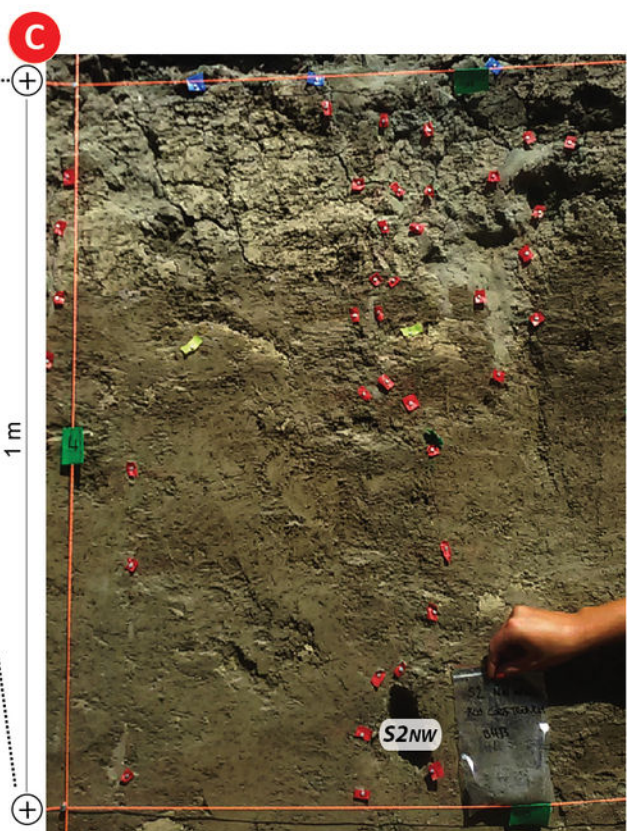
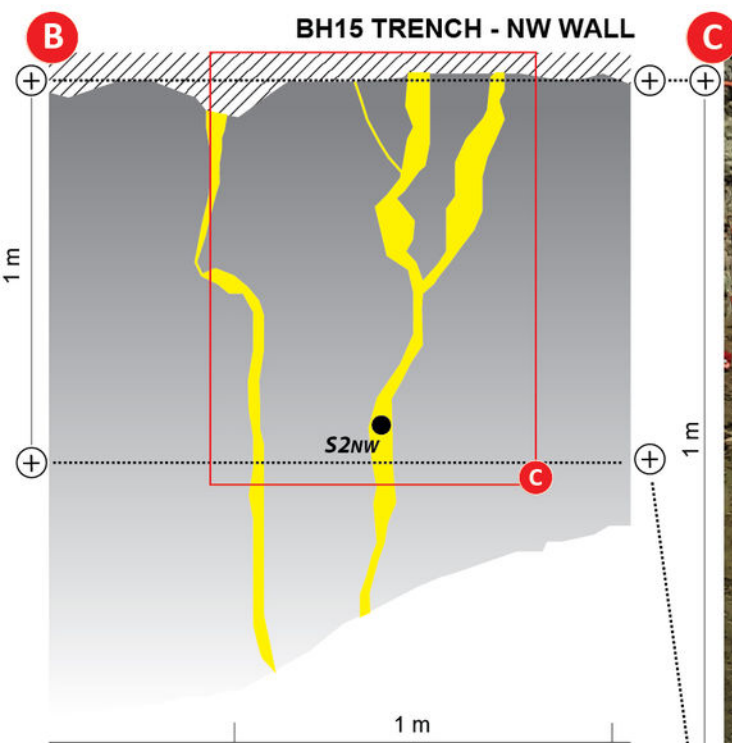


- | | | | | | |
|---|--|--|---|---|---|
|  Late Holocene channel sand and silty sand |  Mid and late Holocene levee silt and silty sand |  Mid and late Holocene, interfluvial swamp mud |  Early Holocene fluvial silt and sand |  LGM fluvial sand |  anthropic embankment |
|---|--|--|---|---|---|

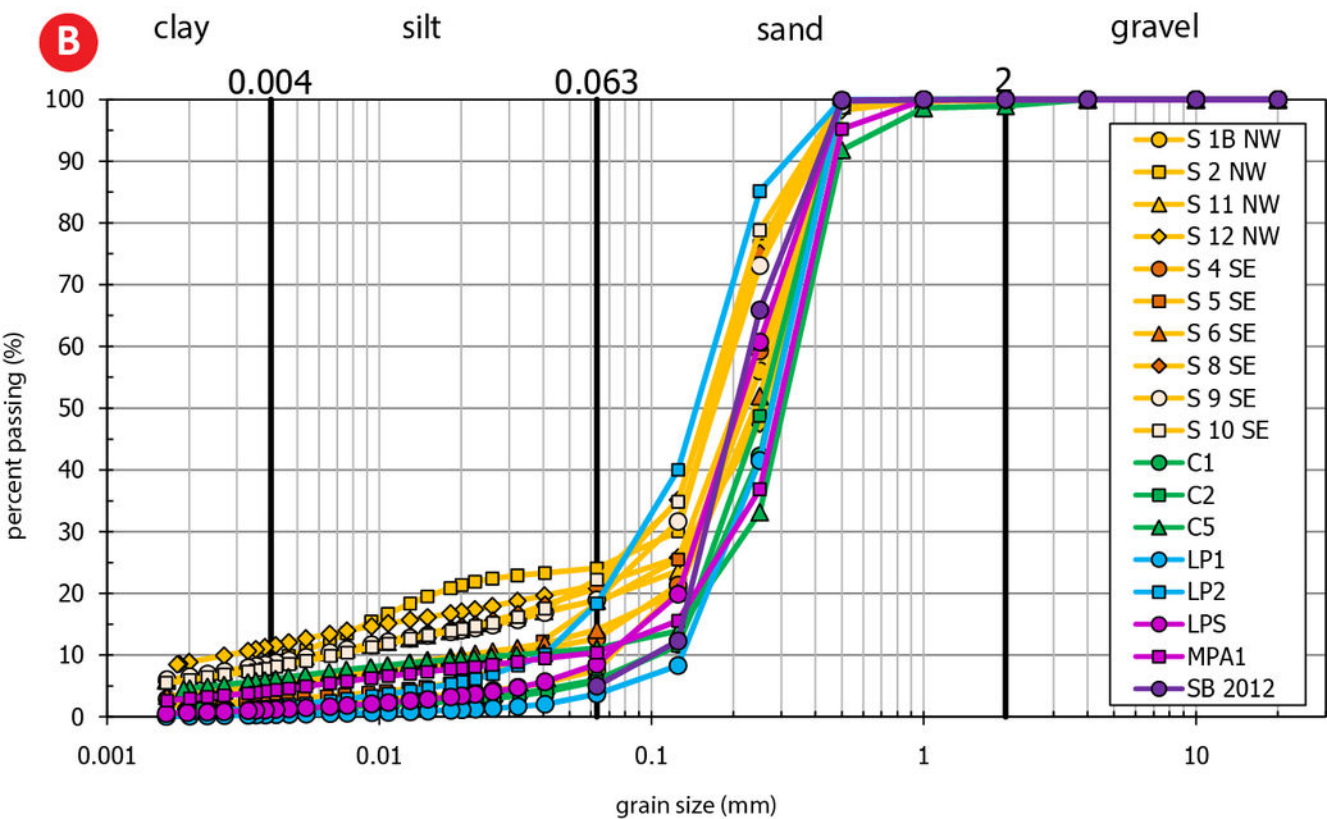
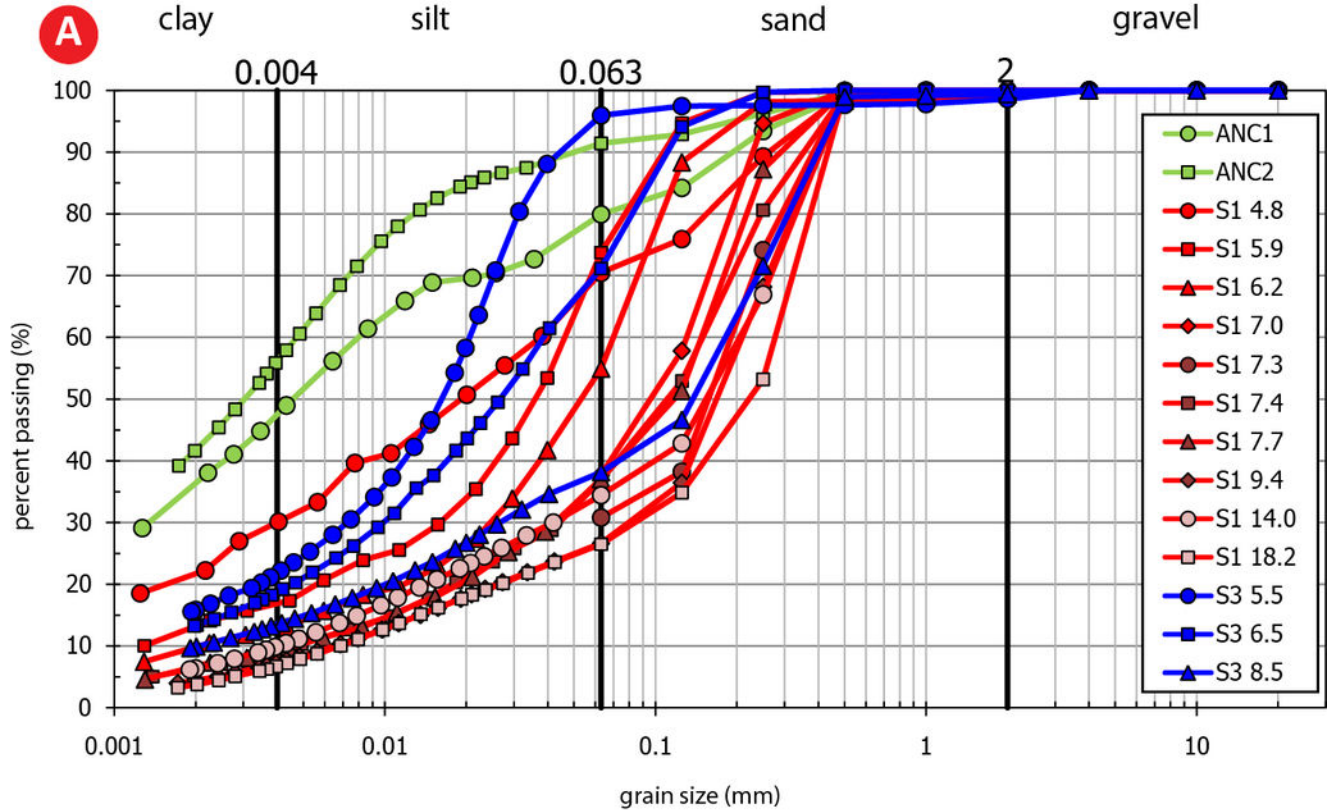


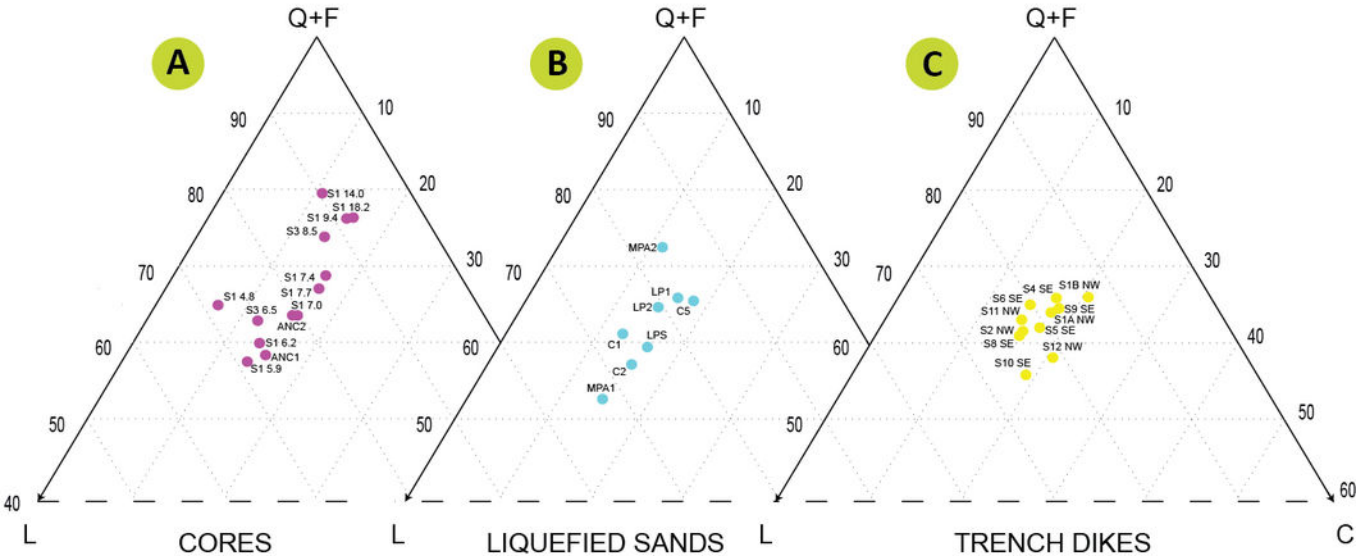
- sand-filled cracks (2012)
- sand boils (2012)
- blast-induced sand boils (C)
- * micropile
- blast area
- - - trace of subsurface profile
- X CPTu
- ▲ settlement profilometer (MP)
- borehole (S)
- trench

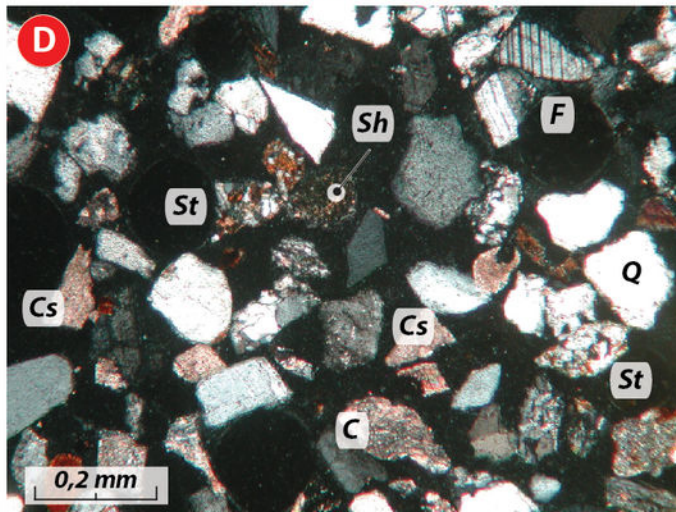
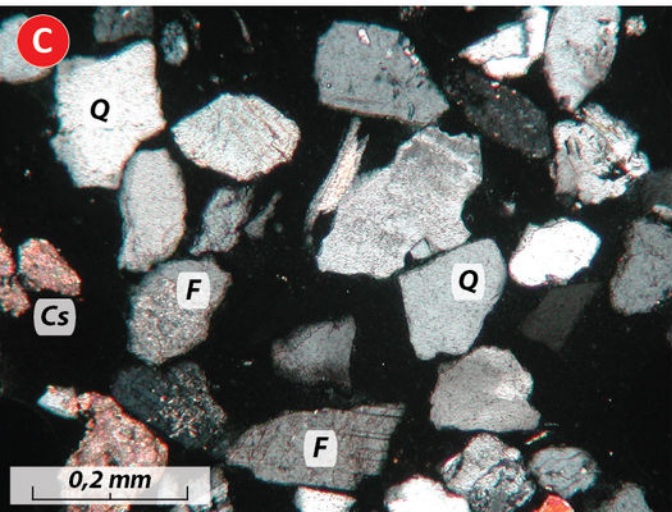
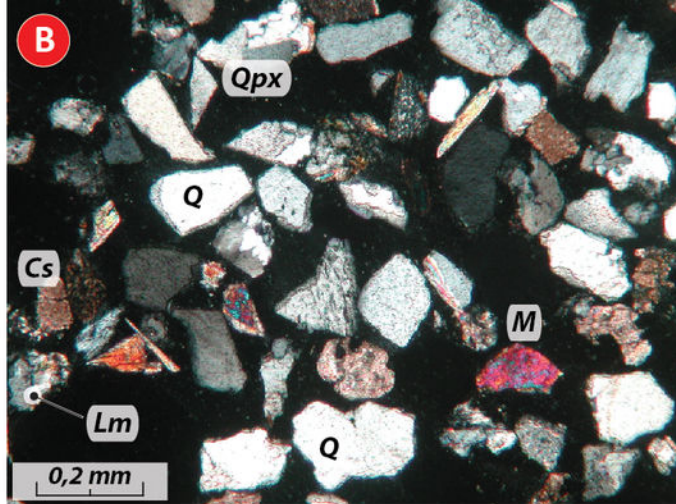
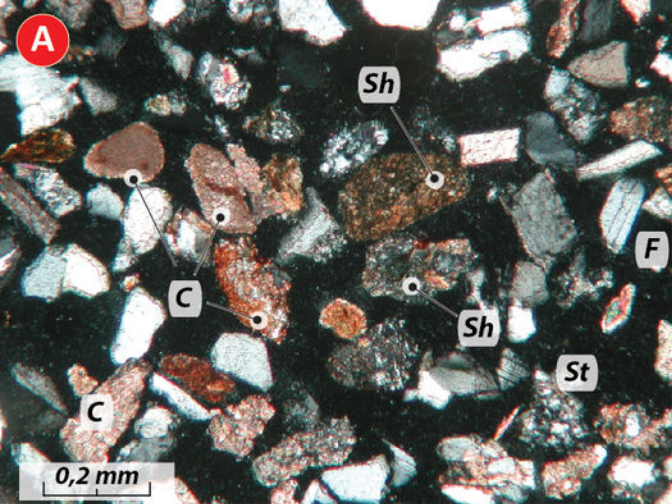


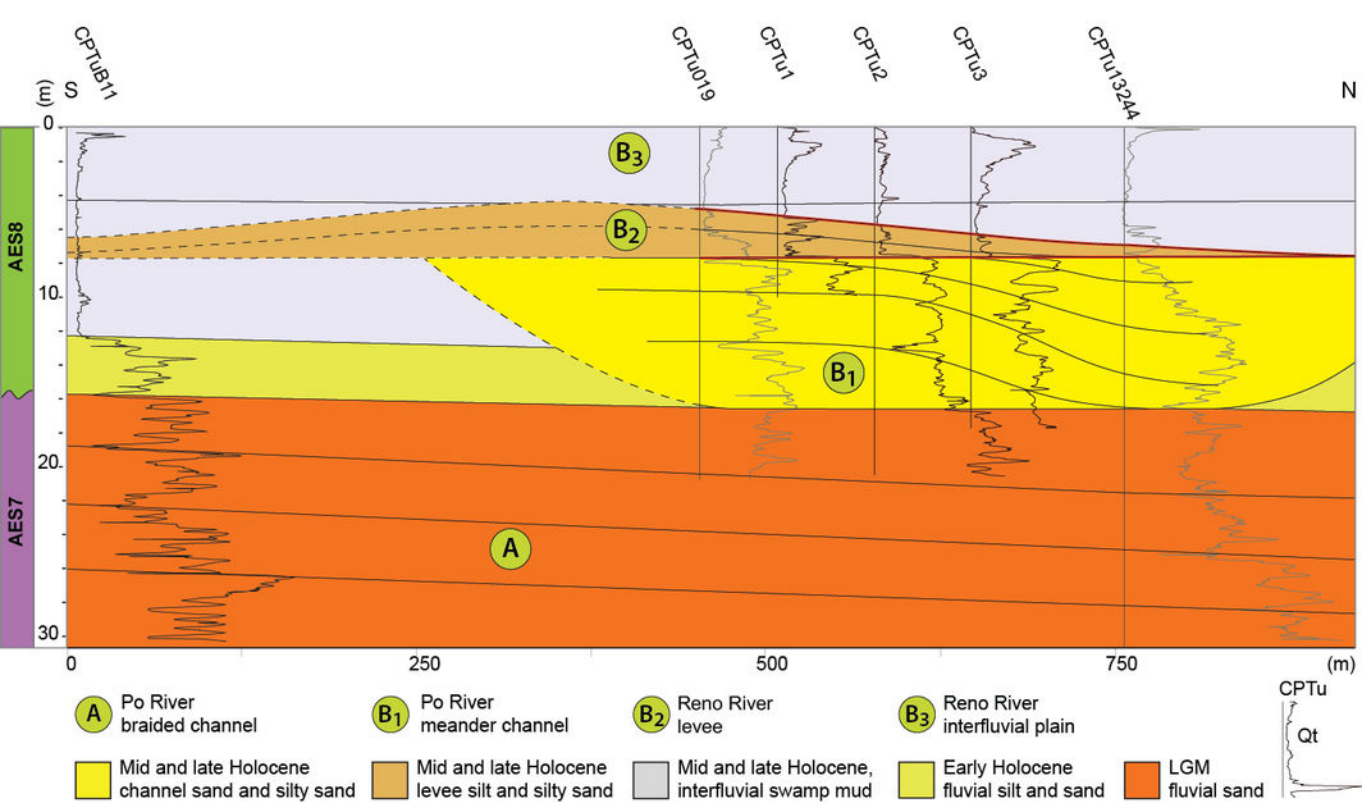


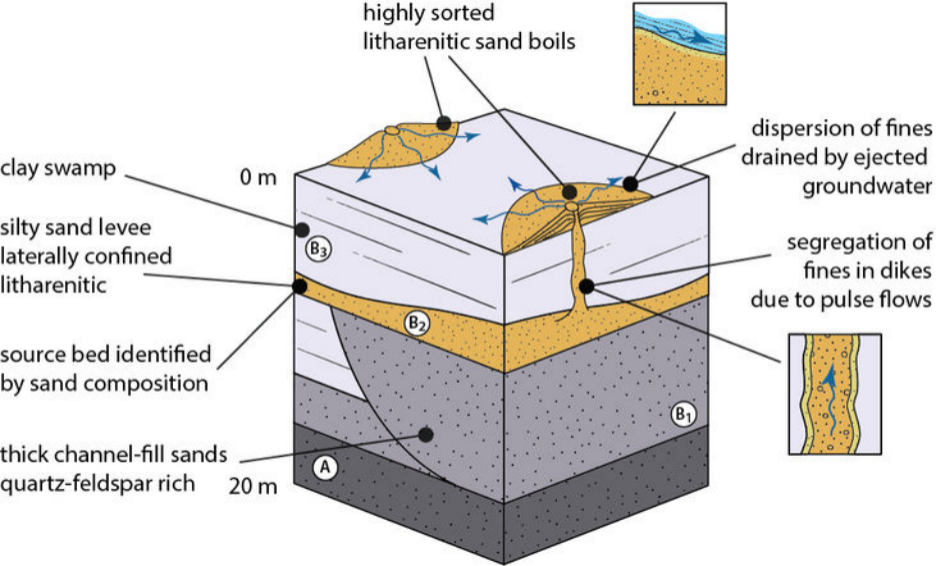
- location of sample S2 NW
- crack filled with sand liquefied during 2012 earthquake
- ▨ reworked material by agricultural practices











| Samples | Description | FC (%) | D ₆₀ (mm) | D ₃₀ (mm) | D ₁₀ (mm) | U | C |
|---------|--------------------------------|--------|----------------------|----------------------|----------------------|-------|------|
| Anc 1 | Anchor of CPTu2 piezocone test | 80.75 | 0.0081 | 0.0014 | - | - | - |
| Anc 2 | Anchor of CPTu2 piezocone test | 91.67 | 0.0047 | - | - | - | - |
| S1 4.8 | Borehole S1 4.8-4.9 m | 71.52 | 0.0378 | 0.0040 | - | - | - |
| S1 5.9 | Borehole S1 5.9-6.1 m | 77.81 | 0.0473 | 0.0161 | 0.0013 | 36.6 | 4.2 |
| S1 6.2 | Borehole S1 6.2-6.3 m | 61.40 | 0.0724 | 0.0248 | 0.0021 | 34.6 | 4.1 |
| S1 7.0 | Borehole S1 7.0-7.3 m | 41.62 | 0.1325 | - | - | - | - |
| S1 7.3 | Borehole S1 7.3-7.4 m | 32.24 | 0.2008 | - | - | - | - |
| S1 7.4 | Borehole S1 7.4-7.5 m | 39.99 | 0.1570 | 0.0447 | 0.0047 | 33.1 | 2.7 |
| S1 7.7 | Borehole S1 7.7-7.8 m | 39.80 | 0.1552 | 0.0434 | 0.0046 | 33.4 | 2.6 |
| S1 9.4 | Borehole S1 9.4-9.5 m | 28.52 | 0.2178 | 0.0843 | 0.0066 | 33.1 | 5.0 |
| S1 14.0 | Borehole S1 14.0-14.1 m | 36.05 | 0.2141 | 0.0420 | 0.0040 | 53.2 | 2.0 |
| S1 18.2 | Borehole S1 18.2-18.3 m | 28.12 | 0.2868 | 0.0890 | 0.0068 | 42.1 | 4.1 |
| S3 5.5 | Borehole S3 5.5-5.6 m | 96.20 | 0.0206 | 0.0073 | - | - | - |
| S3 6.5 | Borehole S3 6.5-6.6 m | 75.59 | 0.0388 | 0.0099 | - | - | - |
| S3 8.5 | Borehole S3 8.5-8.6 m | 39.80 | 0.1921 | 0.0268 | 0.0021 | 93.4 | 1.8 |
| S 1B NW | BH15 trench 0.2 m | 10.15 | 0.2726 | 0.1574 | 0.0743 | 3.7 | 1.2 |
| S 2 NW | BH15 trench 1.4 m | 25.26 | 0.2059 | 0.1245 | 0.0047 | 43.4 | 15.8 |
| S 4 SE | BH15 trench 0.2 m | 14.37 | 0.2543 | 0.1534 | 0.0306 | 8.3 | 3.0 |
| S 5 SE | BH15 trench 1.3 m | 19.73 | 0.2489 | 0.1410 | 0.0339 | 7.3 | 2.4 |
| S 6 SE | BH15 trench 0.5 m | 15.29 | 0.2922 | 0.1636 | 0.0201 | 14.6 | 4.6 |
| S 8 SE | MPA4 trench 0.3 m | 23.62 | 0.2028 | 0.1027 | 0.0060 | 33.9 | 8.7 |
| S 9 SE | MPA4 trench 0.6 m | 21.40 | 0.2105 | 0.1169 | 0.0059 | 35.7 | 11.0 |
| S 10 SE | MPA4 trench 1.6 m | 24.71 | 0.1965 | 0.1011 | 0.0068 | 28.7 | 7.6 |
| S 11 NW | MPA4 trench 2.2 m | 19.76 | 0.3029 | 0.1557 | 0.0057 | 53.4 | 14.1 |
| S 12 NW | MPA4 trench 2.0 m | 22.22 | 0.3118 | 0.1493 | 0.0028 | 113.1 | 25.9 |
| C1 | Blast sand boil | 7.13 | 0.3271 | 0.1998 | 0.1058 | 3.1 | 1.2 |
| C2 | Blast sand boil | 6.89 | 0.3051 | 0.1870 | 0.1085 | 2.8 | 1.1 |
| C5 | Blast sand boil | 11.70 | 0.3643 | 0.2294 | 0.0320 | 11.4 | 4.5 |
| LP1 | Micropile sand boil | 4.61 | 0.3292 | 0.2066 | 0.1313 | 2.5 | 1.0 |
| LP2 | Micropile sand boil | 22.54 | 0.1803 | 0.0963 | 0.0399 | 4.5 | 1.3 |
| LPS | Micropile trench | 10.70 | 0.2477 | 0.1560 | 0.0710 | 3.5 | 1.4 |
| MPA1 | MPA1 profilometer trench | 11.43 | 0.3490 | 0.2097 | 0.0523 | 6.7 | 2.4 |
| SB 2012 | 2012 Sand boil | 7.30 | 0.250 | 0.175 | 0.095 | 1.4 | 0.7 |

